Image Watermarking Scheme Based on 3-D SWT

WANG Jin-wei, LIU Guang-jie, DAI Yue-wei, WANG Zhi-quan

(*Department of Automation, Nanjing University of Science and Technology, Nanjing* 210094)

Abstract Robust watermarking techniques are always used for copyright protection and ownership assertion. Many watermark embedding schemes in transform domain are proposed such as 2-D DFT, 2-D DCT and 2-D DWT which are used to transform the image data, and 3-D DCT and 3-D DWT which are used to transform the video data and 3-D image data. In this paper, a gray-level image watermarking scheme based on 3-D separable wavelet transform(SWT) with lifting scheme is presented. A gray-level image is decomposed into a 3-D image sequences by sub-sample of zigzag scan which are transformed using 3-D SWT. Simultaneously it is proved that the distribution of 3-D SWT coefficients follow the generalized Gaussian density function by using the distribution relative entropy theory. To make the compromise between the robustness and the imperceptivity, a new 3-D HVS model is reconstructed and used to adjust the embedding strength. In watermark detection, the optimum detector is used to implement the blind detection. It is shown in our experiments that the scheme is strongly robust against various attacks.

Keywords digital watermark, lifting wavelet, HVS, relative entropy, optimum detection

基于 3 维提升可分离小波变换的图像水印方案

王金伟 刘光杰 戴跃伟 王执铨

(南京理工大学自动化系，南京 210094)

摘 要 鲁棒水印技术通常被用于版权保护和所有权声明等目的。许多提出的水印方案通常把水印嵌入在变换域内，如 2 维的 DFT 域、DCT 域和 DWT 域以及 3 维的 DCT 域、WT 域。前 3 个域主要被用于 2 维的图像载体，而后 2 个域主要被用于 3 维的视频载体和 3 维的图像载体。在本文中，一种基于 3 维提升可分离小波(3-D SWT)的灰度图像水印方案被提出。首先，通过之字扫描把灰度图像分解为 3 维的图像序列，然后使用 3-D SWT 变换这些图像序列。同时通过相对熵理论证明了 3-D SWT 变换系数符合广义高斯分布。为了平衡鲁棒性和不可感知性，新的适用于 3 维的人类视觉模型被重构并用于调整水印的嵌入强度。在水印的检测方面，最优检测器实现水印的盲检测。实验表明本方案对各种攻击是强鲁棒的。

关键词 数字水印 提升小波 人类视觉模型 相对熵 最优检测

中图法分类号：TP391 TP309 **文献标识码**：A **文章编号**：1006-8961(2007)03-0413-07

1 Introduction

In recent years, more and more digital data can be easily transmitted, duplicated and modified through the Internet which caused unauthorized copying and distribution. Therefore, the copyright protection of the intellectual property of the digital data is becoming an important legal issue. Digital watermarking is considered as a possible solution for copyright protection. Watermarking techniques are rapidly developed up to now.

However, all watermarking schemes must satisfy three basic requirements: imperceptivity which means

基金项目：国家自然科学基金项目(60374066)，江苏省自然科学基金项目(BK2002101)

收稿日期：2005-09-06；**改回日期**：2005-12-02

第一作者简介：王金伟(1978～)，男。南京理工大学自动化学院博士研究生。主要研究方向为数字水印、多媒体认证、信号处理。E-mail：wjwei_2004@163.com

the statistical distribution of the watermarked image is similar to that of the original image, robustness which means the capability against various attacks such as JPEG compression, cropping, low-pass filtering and so on, and security which means the capability against the unauthorized and illegal attacks.

At present though large amounts of watermarking schemes have been proposed, they can be classified into two categories. One category is that watermark is embedded in spatial domain, for example, LSB scheme[1]. However, this sort of the watermarking schemes is fragile against the attacks, in particular, low-pass filtering. The other is to embed watermark in transform domain such as in DFT, DCT, and DWT domain[2~4]. These schemes in 2-D transform domain mainly embed watermark into image data or each frame of video data and those in 3-D transform domain almost embed watermark into 3-D video data or 3-D image data[5,6].

In [7], the author proposed a watermarking scheme based on sub-sampling. The main idea of the scheme is that the original image is divided into four sub-images after the sub-sampling and then the sub-images are respectively transformed using DWT to embed watermark by analyzing the relation between the coefficients of two sub-images. The disadvantage of the scheme is that the watermark can not diffuse each pixel in original image. A wavelet-based scheme proposed in [8] uses the HVS model to implement the balance between the robustness and the imperceptivity, but the watermark detector requires the original image.

In this paper, we propose the watermarking scheme which the gray-level images are transformed using 3-D SWT with lifting scheme.

2 Decomposing Image

We need extend a 2-D image to a 3-D sub-image sequence. The process of decomposing image needs satisfy two important requirements. One is the dependence among the pixels of a sub-image and the other is the relativity between two sub-images. For satisfying the first requirement, the size of sub-sampling blocks must be moderate. We use the zigzag scan to meet the second requirement.

The decomposition of an image includes the following steps.

(1) An original image whose size is $M \times N$ is divided into $(M/m) \times (N/n)$ blocks whose size is $m \times n$.

(2) Each block is scanned by the form of zigzag and then converted into a $l = m \times n$ vector. The vector forms the third dimension similar to the time axis in video. The process of zig-zag scan is depicted in Figure 1.

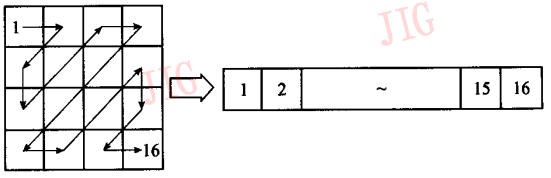

Fig. 1 Scanning block

(3) The original image is decomposed into a 3-D $(M/m) \times (N/n) \times l$ sub-image sequences.

It is assumed that the size of the original image is 512×512. Let $m = n$ be equal to 4 here for satisfying the first requirement. Then we get a 3-D $128 \times 128 \times 16$ sub-image sequence. In Figure 2, the process of decomposing image is depicted.

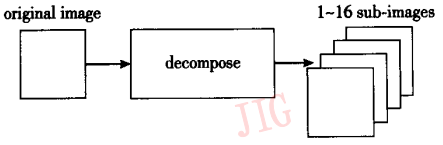

Fig. 2 Block of decomposing image

3 Distribution Fitness of 3-D SWT

The basic information measure of hypothesis testing is the relative entropy between two probability distributions $p(x)$ and $q(x)$[2], defined as

$$RE = \sum_{i=0}^{l-1} p_i(x) \log \frac{p_i(x)}{q_i(x)} \quad (1)$$

The relative entropy between two distributions is nonnegative and is 0 if and only if the distributions are equal. Therefore, it can be used to measure the similarity between two distributions. Two distributions tend to be the same with the relative entropy

decreasing[2].

The sub-image sequence in Section 2 is decomposed into 3 resolution levels using 3-D SWT with lifting scheme. In the first and the second level, there are respectively seven detail matrices and in the third level there are one approximation matrix and seven detail matrices. Figure 3 shows the decomposition of 3-D SWT and the shaded areas in Figure 3 depict seven detail matrices in the second level.

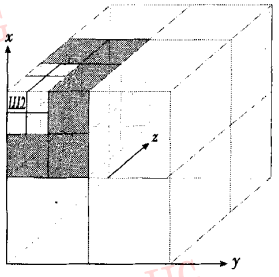

Fig. 3　The decomposition of 3-D SWT

Through the experiments we prove that the distribution of seven detail matrices in the second level follows the generalized Gaussian distribution using the relative entropy.

The probability density function of the generalized Gaussian distribution is

$$f(x) = A \cdot \exp(-|\beta(x-m)|^{\rho}) \tag{2}$$

$$A = \frac{\beta\rho}{2\Gamma(1/\rho)} \tag{3}$$

$$\beta = \frac{1}{\sigma}\left(\frac{\Gamma(3/\rho)}{\Gamma(1/\rho)}\right)^{1/2} \tag{4}$$

where $\Gamma(x) = \int_0^{+\infty} t^{x-1}e^{-t}dt$ is the Gamma function, m and σ^2 are respectively the expectation and the variance of the distribution. The power of the exponent ρ is the shape parameter. The GGD model contains the Laplacian and the Gaussian distributions as special cases, with $\rho=1$ and $\rho=2$, respectively.

In this paper, the probability distribution of 3-D SWT coefficients is denoted as $p(x)$, and the probability distribution of fitting 3-D SWT coefficients is denoted as $q(x)$.

In our experiments, a large number of images are transformed using 3-D SWT with lifting scheme. Figure 4 shows the matching graphics of two distributions $p(x)$ and $q(x)$ of Baboon image. The values of relative entropy between two distributions $p(x)$ and $q(x)$ are listed in Table 1. The small values of relative entropy between two distributions in Table 1 prove that the distribution of 3-D SWT coefficients obeys the generalized Gaussian distribution.

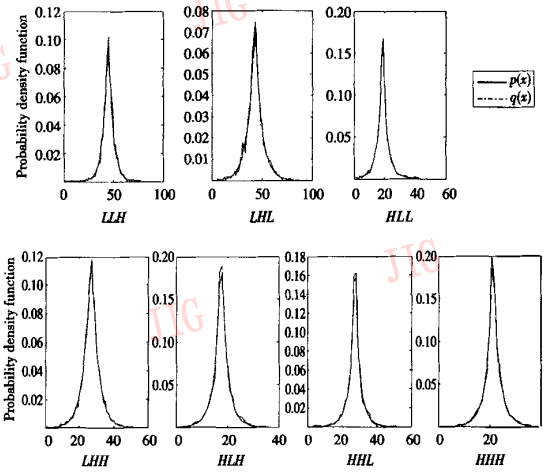

Fig. 4　Matching graphics between two distributions $p(x)$ and $q(x)$

Tab. 1　Value of relative entropy between $p(x)$ and $q(x)$

Name	*LLH*	*LHL*	*HLL*	*LHH*	*HLH*	*HHL*	*HHH*
Baboon	0.025	0.019	0.034	0.011	0.026	0.039	0.026
Elaine	0.062	0.055	0.052	0.070	0.12	0.21	0.009
Goldhill	0.025	0.046	0.016	0.039	0.040	0.021	0.051

4　3-D HVS model

The quantization model based on 2-D HVS proposed in[9,10] is not fit for the 3-D wavelet coefficients. Hence we improve the quantization model to reconstruct 3-D HVS model to fit for 3-D SWT coefficients.

$I^{(r,s)}(x,y,z)$ is the coefficient value of the decomposition I at level $r=0,1,2$, orientation $s \in \{LLL, LLH, LHL, HLL, LHH, HLH, HHL, HHH\}$, and position x, y, z within that sub-band. The following equations are improved to fit for 3-D SWT coefficients according to [9].

$$T(r,s,x,y,z) = frequncy(r,s) * luminance(r,x,y,z) * texture(r,x,y,z)^{0.034} \tag{5}$$

Band sensitivity depends on the change of band, especially the orientation and the level of detail

matrix[10].

$$frequency(r,s)=\begin{Bmatrix}\sqrt{3}, & \text{if } s=HHH\\ \sqrt{2}, & \text{if } s=LHH,HLH,HHL\\ 1, & \text{if } s=LLH,LHL,HLL\end{Bmatrix}*\begin{Bmatrix}1.00 & \text{if } r=0\\ 0.32 & \text{if } r=1\\ 0.16 & \text{if } r=2\end{Bmatrix} \tag{6}$$

The human eye is less sensitive to noise for brighter background. The lower-pass coefficients can be used to represent background luminance[9,10]. Taking account of the luminance masking equation is given as follows:

$$luminance(r,x,y,z)=1+\frac{1}{256}\sum_{i=0}^{1}\sum_{j=0}^{1}\sum_{k=0}^{1}I^{2,LLL}(i+1+x/2^{2-r},\ j+1+y/2^{2-r},k+1+z/2^{2-r}) \tag{7}$$

Texture masking decreases the sensitivity to noise if there is high activity in the locality of the coefficient. The energy of lower frequency coefficients can indicate the texture activity level[9].

$$\begin{aligned}texture(r,x,y,z)=&\sum_{i=1}^{2-r}16^{-l}\sum_{s\neq LLL}\sum_{i=0}^{1}\sum_{j=0}^{1}\sum_{k=0}^{1}(I^{l+r,s}(i+x/2^{l},\\ &j+y/2^{l},k+z/2^{l}))^2+\\ &16^{2-l}var(I^{2,LLL}(\{1,2\}+x/2^{2-r},\\ &\{1,2\}+y/2^{2-r},\{1,2\}+z/2^{2-r}))\end{aligned} \tag{8}$$

The equation is composed of the sum of two terms. The first term represents the edges distance, while the second one represents the texture activity.

We use the reconstructed HVS model to adjust the watermarking strength embedding into the original image. The watermarked image keeps high fidelity. The difference between the original image and the watermarked one is shown in Figure 5. Figure 5 explains that the 3-D HVS model reconstructed by us can adaptively adjust the watermark embedding strength according to the content of an image.

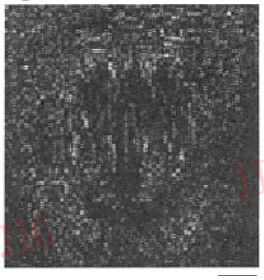

Fig. 5 The difference between original image and watermarked image

5 Embedding and Detection

An original image is first decomposed into a 3-D 128 × 128 × 16 sub-image sequence according to Section 2. Then the 3-D sub-image sequence is decomposed into three levels using 3-D SWT with the lifting scheme. To adaptively embed a sequence of watermark, we use the 3-D HVS model in Section 4 to analysis the 3-D SWT coefficients. The block of watermark embedding process is shown in Figure 6.

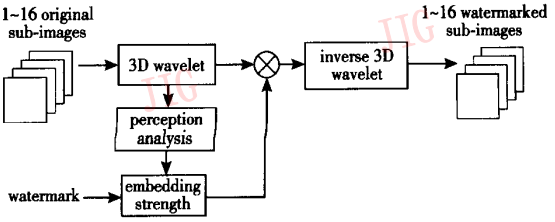

Fig. 6 Adaptively watermarking block

Let the components of the watermarks from the 3-D matrix $\boldsymbol{W}$ follow the uniform distribution in $[-1,1]$. The rule of watermark embedding is as follows:

$$I'^{(r,s)}(x,y,z)=\begin{cases}I^{(r,s)}(x,y,z)(1+\alpha(x,y,z)W(x,y,z)) & \text{if } r=1,s\neq LLL\\ I^{(r,s)}(x,y,z) & \text{otherwise}\end{cases} \tag{9}$$

Where

$$\alpha(x,y,z)=\alpha\times T(x,y,z)$$

$I'^{(r,s)}(x,y,z)$ is $I^{(r,s)}(x,y,z)$ corresponding watermarked coefficient and α is a constant scaling factor. $T(x,y,z)$ is a weighting function.

To detect the watermark without original image, we evaluate the response of watermark detector using the optimum detection scheme[11] which uses the hypotheses test principle. In fact, the optimum detection is a likelihood ratio test in the sense of Neyman-Pearson Lemma[12].

First, two hypotheses are established as follows[11]:

$$H_0:\alpha(x,y,z)=0$$

$$H_1:\alpha(x,y,z)>0$$

If the watermark is proved to be existing, which means the watermark embedding strength is not equal to zero and the optimum detector $z(I)$ is greater than the decision threshold η, H_1 is accepted, or H_0 is

accepted. The equations of optimum detector $z(I)$ and the decision threshold η are respectively listed[11].

$$z(I') = \frac{1}{N}\sum_{s\neq LLL}\rho_{1,s}\,|\beta_{1,s}|^{\rho_{1,s}}\sum_x\sum_y\sum_z |I^{(1,s)'}(x,y,z)|^{\rho_{1,s}}W(x,y,z) \tag{10}$$

$$\eta = \sqrt{2}\sigma_z erfc^{-1}(2\bar{P}_{fp}) + \mu_z \tag{11}$$

$$\mu_z = \frac{1}{N}\sum_{s\neq LLL}\sum_x\sum_y\sum_z W(x,y,z) \tag{12}$$

$$\sigma_z^2 = \frac{1}{N^2}\sum_{s\neq LLL}\rho_{1,s}\sum_x\sum_y\sum_z W(x,y,z)^2 \tag{13}$$

where N is the total number of the 3-D SWT coefficients to which are added the watermark, and $\rho_{1,s}$ represents the shape parameter of GGD at level $r=1$, orientation $s \in \{LLL, LLH, LHL, HLL, LHH, HLH, HHL, HHH\}$.

$$erfc(x) = \frac{2}{\sqrt{\pi}}\int_0^{+\infty}\exp(t^2)\,dt$$

$$\bar{P}_{fp} = \frac{1}{2}erfc\left(\frac{\eta_l - \mu_z}{\sqrt{2}\sigma_z}\right)$$

In [11], the deduction process is described in detail.

6 Experiments

To analyze the performance of the scheme proposed in this paper, we use the original images whose size is 512 × 512 in the experiment. Here we only list the experimental results of the original image "Baboon". The various attacks are applied to the watermarked image to evaluate the robustness. The comparison between the original image and the watermarked image is shown in Figure 7. The human eye cannot distinguish between the original image and the watermarked image.

6.1 JPEG Lossy Compression

It is known that the image fidelity decreases with the quality factor decreasing. When the quality factor is 0, the image distortion is heaviest. When the quality factor is 100, the image has no distortion. We perform the JPEG compression with quality factors decreasing every 5 from 100 to 0. It is observed in Figure 8 that the optimum detector cannot detect watermark from compression image with quality factor close to 0. Therefore, the scheme is resilient against JPEG compression attack.

(a) Original image　　(b) Watermarked image

Fig. 7　Comparison of Original image and watermarked image

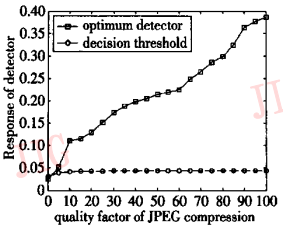

Fig. 8　Optimum detection under JPEG compression attack

6.2 Adding Gaussian Noise

Gaussian noise is added to the watermarked image to evaluate the robustness of resisting noise. The Gaussian noise variance in simulation increases every 5.1 from 0 to 51. We observe from Figure 9(a) that the optimum detector is lower than the decision threshold when the noise density is above 45.9. Figure 9(b) is the watermarked image polluted by the Gaussian noise whose density is 40.8. It is obvious that the watermark can be still detected correctly though the watermarked image is heavily destroyed as shown in Figure 9(b).

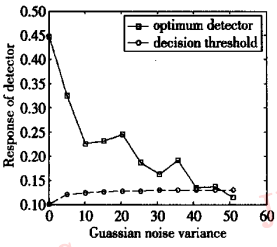

(a) Response of optimum detector　　(b) Polluted image

Fig. 9　Optimum detection under adding-Gaussian-noise attack

6.3 Cropping

The detector cannot detect watermark correctly because of cropping attack making the content of

watermarked image lost. The step size of cropping image is 16 pixels. We increase step size from 16 pixels to 160 pixels. The row size of cropped image is $(512-2\times160)=192$ pixels. The response of optimum detector given in Figure 10(a) depicts that the scheme is strongly robust against cropping attack. The cropped watermarked image of size 192×192 is shown in Figure 10(b).

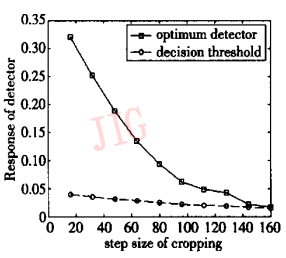

(a) Response of optimum detector

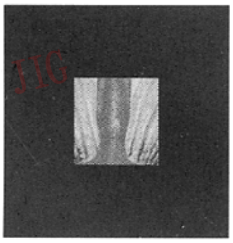

(b) Polluted image

Fig. 10 Optimum detection under cropping attack

6.4 Low-Pass Filtering

To valuate the resilient against low-pass filtering, the watermarked image is filtered with Gaussian filter of size 4 with standard deviation σ_g. The increment of σ_g is 0.1 from 0 to 2. The graphic of the function between optimum detector and standard deviation σ_g in Figure 11(a) shows that the scheme can resist against low-pass filtering attack. We observe from Figure 11(b) that the watermarked image filtered with standard deviation σ_g equal to 0.16 loses a lot of detail like the face of "Baboon".

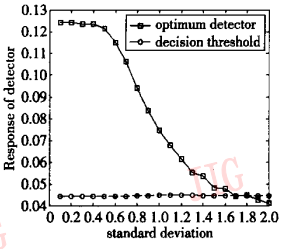

(a) Response of optimum detector

(b) Polluted image

Fig. 11 Optimum detection under low-pass filtering attack

6.5 Valumetric Scaling

Valumetric scaling changes the amplitude of the watermarked image. Volumetric scaling down or up corresponds to the change of brightness and contrast of the image. Two tests are performed here. The factor of volumetric scaling up varies from 1 to 0.1. The factor of volumetric scaling up varies from 1 to 3. The results of volumetric scaling down are summarized in Figure 12 (a). The optimum detector almost remains unchanged. In Figure 13(a) the results of volumetric scaling up depict that the optimum detector rapidly decreases with the volumetric scaling factor increasing, but the watermark is still detected correctly. The results in two figures demonstrate that the scheme is very strongly robust against volumetric scaling-down and volumetric scaling-up attacks. Figure 12 (b) shows the watermarked image corresponding to the volumetric scaling factor equal to 0.5. Figure 13(b) shows that the watermarked image corresponding to the volumetric scaling factor equal to 2.

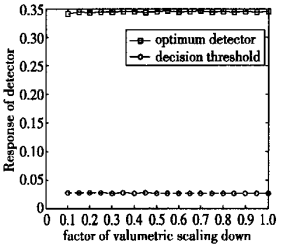

(a) Response of optimum detector

(b) Polluted image

Fig. 12 Optimum detection under volumetric scaling-down attack

6.6 Resizing

Resizing changes the size of the watermarked image. We implement two tests. First, the watermarked image is downsized and then recovered to the original size. Secondly, the size of the watermarked image is increased and then recovered. The results of the first test and the second test are respectively shown in Figure 14 (a) and (b). It is obvious that the results of thesecond test are better than that of the first test because reducing the size of an image makes the image lose more details than increasing the size of the image.

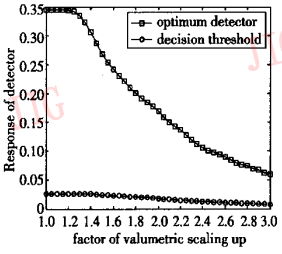

(a) Response of optimum detector

(b) Polluted image

Fig. 13 Optimum detection under volumetric scaling-up attack

6.7 Comparison

For the impartiality of comparison, we use the same PSNR value, the same threshold, the same embedding rule and the same detector in this comparison experiment. The PSNR value and is set to 43.378dB. The embedding rule and the detector are respectively the multiplicative rule and the optimum detector used in this paper. The threshold is normalized to 4.75. Which means that the computation equation (10) of the detection value is modified according to the threshold equation (11). If the detection value of one scheme is bigger than that of another scheme, the performance of the scheme corresponding to big detection value is better.

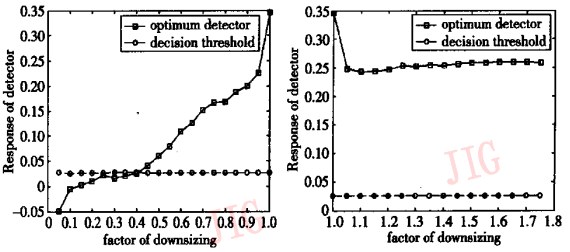

(a) Under downsizing attack　　(b) Under increasing-size attack

Fig. 14　Optimum detection under resizing attack

Now the comparative results between the scheme based on 2-D DWT and our proposed scheme is listed in Table 2. Judged from Table 2, our proposed scheme gets an advantage over the scheme based on 2-D DWT.

Tab. 2　Comparative Results between the scheme based on 2-D DWT and our proposed scheme

	JPEG(50)	Gaussian noise	Cropping	Low pass	Valumetric Scaling-up	Valumetric Scaling-down	Resizing
2-D DWT	17.20	18.90	16.59	7.15	19.77	19.82	18.4
Our scheme	18.3	25.57	27.85	5.57	30.34	30.3	22.7

7 Conclusion

In this paper, we decompose a 2-D image to a 3-D sub-image sequence. The sub-image sequence is transformed using 3-D SWT with lifting scheme and used the reconstructed 3-D HVS model to adaptively embed the watermark. The experiments prove that the 3-D HVS model can get good visual effect.

The optimum detector is adapted to realize the watermark detection without original image.

It is shown in the experiments that the scheme is resilient against various attacks such as JPEG compression, contaminating by Gaussian noise, cropping, low-pass filtering, scaling and resizing and so on. The comparison results prove that our proposed scheme based on 3-D SWT excels the schemes based on 2-D DWT.

References

1 Liu S, Chen T, Yao H, *et al*. A variable depth LSB data hiding technique in images[A]. In: Proceedings of IEEE International Conference on Machine Learning and Cybernetics[C], Shanghai, China, 2004, **7**: 3990~3994.

2 Cachin C. An information-theoretic model for steganography[A]. Portland: The 2nd Workshop on Information Hiding[C], Oregon, USA, 1998, **1524**: 306~318.

3 Solachidis V, Pitas I. Circularly symmetric watermark embedding in 2-D DFT domain[J]. IEEE Transactions on Image Processing, 2001, **10**(11): 1741~1753.

4 Suhail M, Obaidat M. Digital watermarking-based DCT and JPEG model[J]. IEEE Transactions on Instrumentation and Measurement, 2003, **52**(5): 1640~1647.

5 Kim S, Lee S, Kim T, *et al*. A video watermarking using the 3-D wavelet transform and two perceptual watermarks[A]. In: International Workshop on Digital Watermark[C], South Korea, Seoul, 2004: 329~338.

6 Wu Y, Guan X, Kankanhali M, *et al*. Robust invisible watermarking of volume data using the 3D DCT[A]. In: Computer Graphics International[C], Hong Kong, China, 2001: 359~362.

7 Tsai M, Hung H. DCT and DWT-based image watermarking by using sub-sampling[A]. In: The 24th International Conference on Distributed Computing Systems Workshops[C], Tokyo, Japan, 2004: 184~189.

8 Kaewkamnerd N, Rao K. Wavelet based image adaptive watermarking scheme[J]. Electronics Letters, 2000, **36**(4): 312~313.

9 Lewis A, Knowles G. Image compression using the 2-D wavelet transform[J]. IEEE Transactions on Image Processing, 1992, **1**(2): 244~250.

10 Guzmán V, Miyatake M, Meana H. Analysis of a wavelet-based watermarking algorithm[A]. In: Proceedings of the 14th International Conference on Electronic, Communication and Computes[C], Veracruz, Mexico, 2004: 283~287.

11 Kaewkamnerd N, Rao K. Wavelet based image adaptive watermarking scheme[J]. Electronics Letters, 2000, **36**(4): 312~313.

12 Cheng Q, Huang T. Optimum detection of multiplicative watermarks using locally optimum decision rule[A]. In: IEEE International Conference on Multimedia and Expo[C], Japan, Tokyo, 2001: 309~312.